Polymer Vol. 37 No. 13, pp. 2793–2800, 1996

0032-3861/96/$15.00+0.00

Poly(methyl methacrylate) interpenetrating cell model

C. B. Lin
Department of Mechanical Engineering, Tankang University, Tamsui, Taipei Hsien, Taiwan

and Sanboh Lee*
Department of Materials Science, National Tsing Hua University, Hsinchu, Taiwan
(Received 16 February 1995; revised 5 July 1995)

Based on the process of polymerization, an interpenetrating cell model was proposed for poly(methyl methacrylate) (PMMA). This model was used to account for the presence of dimples on the fracture surface of PMMA when voids are present. PMMA was treated by various methods including mixtures of methanol and chlorophyll, gamma irradiation, at different crosshead speeds and after warm drawing. Micrographs taken of the resulting fracture surface morphologies supported the proposed model. Copyright © 1996 Elsevier Science Ltd.

(Keywords: poly(methyl methacrylate); fracture; interpenetrating cell model)

INTRODUCTION

The mechanical properties of poly(methyl methacrylate) (PMMA) have been studied extensively. Chau and Li[1] studied methanol absorption in PMMA shear bands; in these bands the kinetics indicated case I transport. Methanol transport in the deformed PMMA was found to exhibit anomalous behaviour by Harmon *et al.*[2,3]. When irradiated by gamma rays, the molecular chains of PMMA underwent scission so that the molecular weight decreased[4]. The fracture morphology of PMMA was affected by gamma irradiation to the extent that the size of ribs would decrease with increasing gamma ray dosage[5,6]. The rib fracture feature is formed under tensile stress ahead of the crack tip under the action of the applied load[7]. The influence of uniaxial pre-orientation on the craze growth at the crack tip in PMMA and time-dependent relaxation behaviour of the fibril were studied by Könczöl *et al.*[8]. Also, Lin *et al.*[9] investigated the effect of uniaxial pre-orientation on microstructure, e.g. comparing the plastic zone and morphology with the stress intensity factor and angle of switching direction.

Much knowledge of the nature of fracture (or plastic deformation) can be gained from microscopy. Most microscopic analysis has concentrated on crystalline solids including metals and ceramics. For instance, in brittle materials, two parallel cracks join along a line either by secondary cleavage or by shear to form a cleavage step[10]. The merging of cleavage steps results in a river pattern, which has been observed upon grain boundary movement[11]. The cleavage tongue, another feature typical of cleavage fracture in metals, is formed during local fracture along a twin-matrix interface[12]. A tongue was also observed in the shear fracture surface of PMMA in which the microstructure did not exhibit twinning[13]. Dimples in the ductile fracture surface of metals have an irregular shape due to the random occurrence of voids[14]. Puttick[15] and Rogers[16] considered inclusions or intermetallic particles as the initiation sites of voids in metals. However, neither inclusions nor particles exist in glassy polymers, and the reason why dimples form in glassy polymers remains unclear.

A series of studies on the mechanical properties of PMMA and its microstructure[6,9,13,17,18] have recently been reported. This prompted an investigation here of an interpenetrating cell model to account for the dimples in the fracture surface of PMMA when voids are present. Analysis of morphologies produced by methanol/chlorophyll treatment, gamma ray irradiation, variations in crosshead speed and warm drawing supports the proposed model.

INTERPENETRATING CELL MODEL

This model considers the free-radical chain polymerization process applied to amorphous polymers. The flow chart of this model is plotted in *Figure 1*. The initiators and monomers are assumed to be uniformly distributed in the entire space shown in *Figure 1a*. The process of chain initiation involves two steps. First, the initiator I decomposes to yield a pair of free radicals R$^{\cdot}$

$$\mathrm{I} \rightarrow 2\mathrm{R}^{\cdot} \tag{1}$$

and, second, a monomer M adds to a primary radical R$^{\cdot}$ to yield a chain radical $\mathrm{M}_1^{\cdot}$

$$\mathrm{R}^{\cdot} + \mathrm{M} \rightarrow \mathrm{M}_1^{\cdot} \tag{2}$$

The growth of the polymeric molecule occurs via successive addition of a monomer to the radical $\mathrm{M}_x^{\cdot}$

$$\mathrm{M}_x^{\cdot} + \mathrm{M} \rightarrow \mathrm{M}_{x+1}^{\cdot} \tag{3}$$

* To whom correspondence should be addressed

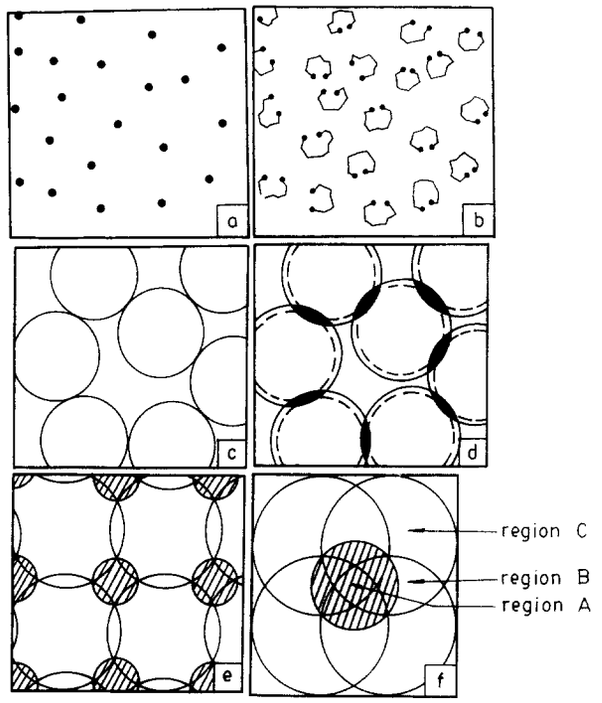

Figure 1 Molecular chain cell model

where x is an integer. The reaction rate is assumed to be independent of chain length. The growth is terminated by the combination

$$M_x^{\cdot} + M_y^{\cdot} \rightarrow M_{x+y} \quad (4)$$

or by disproportionation

$$M_x^{\cdot} + M_y^{\cdot} \rightarrow M_x + M_y \quad (5)$$

The molecular chain is formed in the shape of a deformed circle during the chain reaction as shown in *Figure 1b*. The conversion of monomer to polymer at this stage is about 25%[19]. Meanwhile, the viscosity and polymerization rates increase rapidly. Monomers continue to react with chain radicals in the nucleus of the molecular chain cell. As a result, the molecular chain cell grows until it makes contact with the nearest neighbour cell as shown in *Figure 1c*. At this stage, most of the monomer is attached to the chain radical. The molecular chain is in a gel state. In this highly viscous state the monomer exhibits retarded mobility, thereby leading to a decrease in the polymerization rate. A temperature increase is therefore necessary in order to complete polymerization. Owing to the temperature increase, the molecular chains in the cells become mobile and the cells grow again. Note that the two nearest neighbour cells are close to each other before this stage. The molecular chains reptate and entangle with each other as shown in *Figure 1d*. Monomers continue to react with the chain radical due to the high temperature and low viscosity. Cells overlap with each other so that the molecular chains in one cell penetrate into another, as shown in *Figure 1e*. The degree of entanglement at this stage is greater than that at the previous stage. The degree of entanglement corresponds with the following sequence: corner A > edge B > centre C as shown in *Figure 1f*. When polymer is cooled to about 25°C, the molecular chains shrink and generate residual stresses.

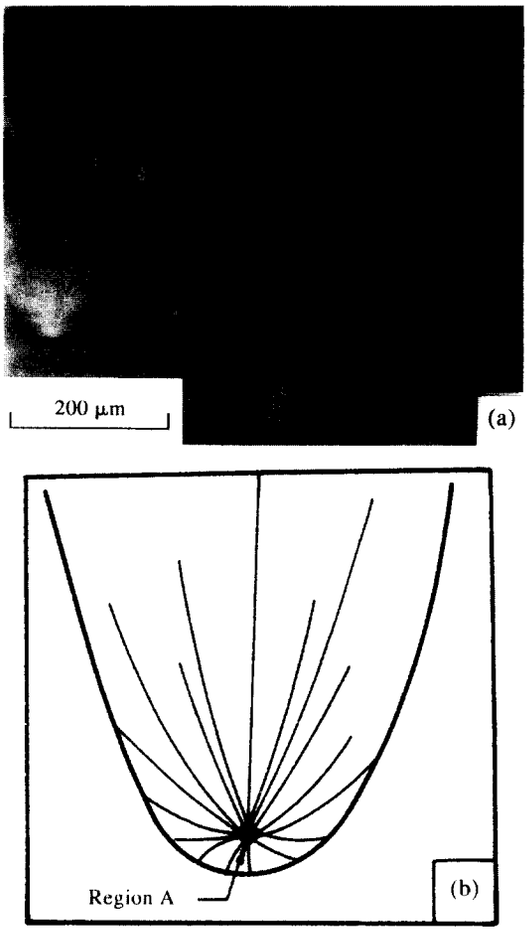

Figure 3 (a) Fractograph of virgin PMMA and (b) the shape of the dimple

EXPERIMENTAL

This work considered solvent treatment, gamma irradiation, strain rate variations and warm drawing. The initial stages of specimen preparation were the same for all studies with the exception of warm drawing. PMMA (Lucite L) with an inherent viscosity of 0.237 was obtained from Du Pont in the form of a 6.1 mm thick cast sheet. Pieces 80 mm × 6.3 mm × 1 mm were cut from

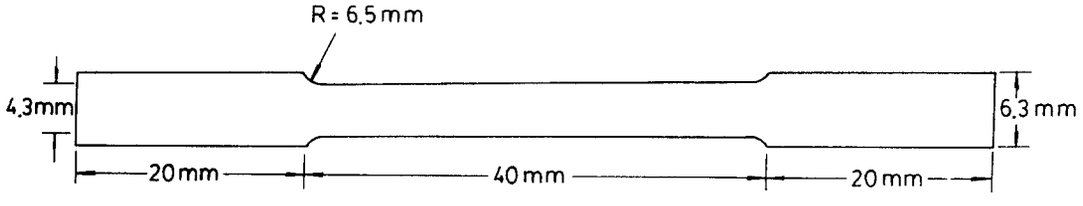

Figure 2 Schematical diagram of a tensile specimen

the cast sheet and then machined into the shape shown in *Figure 2*. These pieces were polished with 600 and 1200 grit carbimet papers and 1 μm and 0.05 μm aluminium slurries. Finally, the specimens were annealed in a vacuum chamber at 120°C for 24 h and furnace-cooled to about 25°C.

Solvent effects

The preweighed samples were preheated to the desired solvent treatment temperature. Each sample was then immersed in methanol mixed with chlorophyll in a stoppered glass bottle, and maintained in a thermostatted water bath at 40–60°C. The volume ratio of methanol to chlorophyll was 10 : 1. The sample absorbed the methanol–chlorophyll mixture until saturation at a given temperature. Samples were removed from the water bath, blotted, and weight gains were recorded. The sample was then desorbed at about 25°C until further weight loss did not occur. The residual amount of methanol mixed with chlorophyll was also recorded. Note that the sample turned a yellowish colour upon desorption: that is, chlorophyll changed to xanthophyll. We assume that chlorophyll accompanies methanol transfer into the specimen. However, when methanol is desorbed, the chlorophyll does not desorb. In other words, the major residual material is chlorophyll. After desorption the specimen was fractured in a tensile tester with a crosshead speed of 0.11 mm min^{-1} at 25°C.

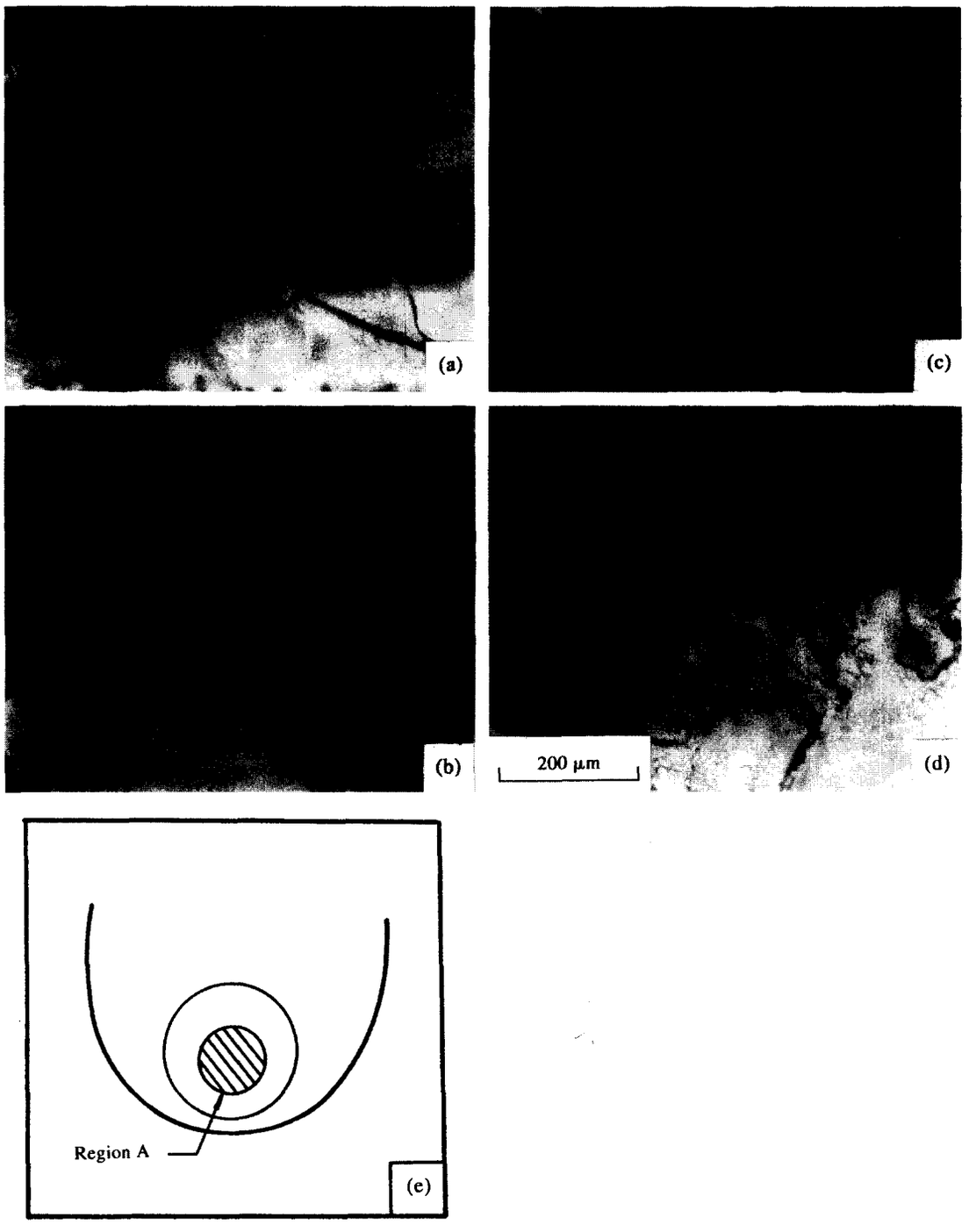

Figure 4 Fractographs of PMMA treated by methanol mixed with chlorophyll at (a) 40, (b) 45, (c) 50 and (d) 55°C. (e) The shape of the dimple in PMMA treated by methanol mixed with chlorophyll

Table 1 Residual amount M of methanol with chlorophyll as a function of treatment temperature T

T (°C)	40	45	50	55	60
M (wt%)	0.0324	0.0359	0.0407	0.0427	0.0501

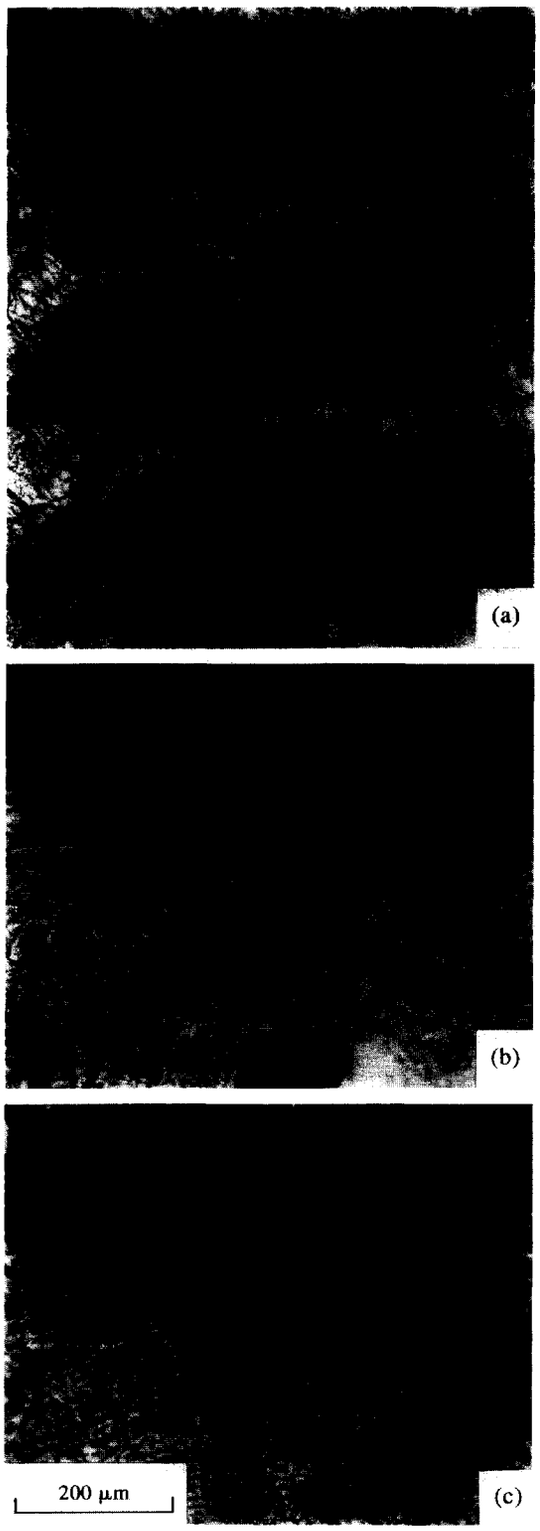

Figure 5 Fracture surface morphology of PMMA irradiated to doses of (a) 10, (b) 20 and (c) 30 Mrad

Fracture morphology was observed using an Olympus BH-2 optical microscope with reflected light.

Gamma ray effects

The samples were exposed in air to gamma radiation from a ^{60}Co source at the Isotope Center in National Tsing Hua University. The dose rate was 1 Mrad h^{-1} at 25°C. The irradiated sample was mounted on the tensile machine and then tested under the action of a tensile load with a crosshead speed of 0.66 mm min^{-1} until fracture. The fracture surface morphology was observed as described above.

Strain rate effects

The sample was fractured in air at 25°C on the tensile machine with various crosshead speeds, and the fracture surfaces observed.

Warm drawing effects

The sample was polished on 1200 grit carbimet paper and then maintained at 110°C in a hot-air furnace. A tensile load was applied with a crosshead speed of 48 mm min^{-1} to produce the desired draw ratio and the sample then cooled down to 25°C in air. The draw ratio was defined as the ratio of drawing length of the sample to the original length. Next, samples of different draw ratios were again polished on 1200 grit carbimet paper to yield the same dimensions, 40 mm × 6.1 mm × 0.5 mm. Final polishing was achieved with 0.05 μm aluminium slurries. The sample was fastened on a vice in order to eliminate recovery, and then immersed in a methanol-filled glass bottle in a thermostatted water bath at 40°C for 30 min. Finally, the morphology was observed using the Olympus BH-2 microscope with transmitted light.

RESULTS AND DISCUSSION

Solvent effects

After annealing, the sample with no solvent treatment (or virgin PMMA) was fractured by applying a tensile load with a crosshead speed of 0.11 mm min^{-1}. A typical fractograph of virgin PMMA exhibits many dimples, as shown in *Figure 3a*. When PMMA is under a tensile load, interpenetrating cells are deformed and the position of highest stress concentration in region A is the final broken point in the cell as shown in *Figure 3b*. With fewer entanglements, chains in region C initially become straightened under the action of the tensile load. When the load increases, chains in region B disentangle and, later, chains in region A follow. This mechanism is different from dimple formation by voids in metals[14]. A comparison of *Figure 3* with *Figure 1* indicates that the size of the chain cell is about 150 μm in diameter.

When PMMA is treated with methanol alone and then desorbed, the fractograph is the same as that of virgin PMMA because the small amount of residual methanol cannot facilitate chain disentanglement[17]. However, when PMMA is immersed in the methanol mixed with chlorophyll until saturation and then desorbed, the fracture surface morphology is different from that of virgin PMMA. Note that no mass uptake of chlorophyll alone in PMMA was observed. The fracture surface morphologies of PMMA with solvent treatment at temperatures of 40, 45, 50 and 55°C are illustrated in *Figures 4a–d*, respectively. The residual amount of

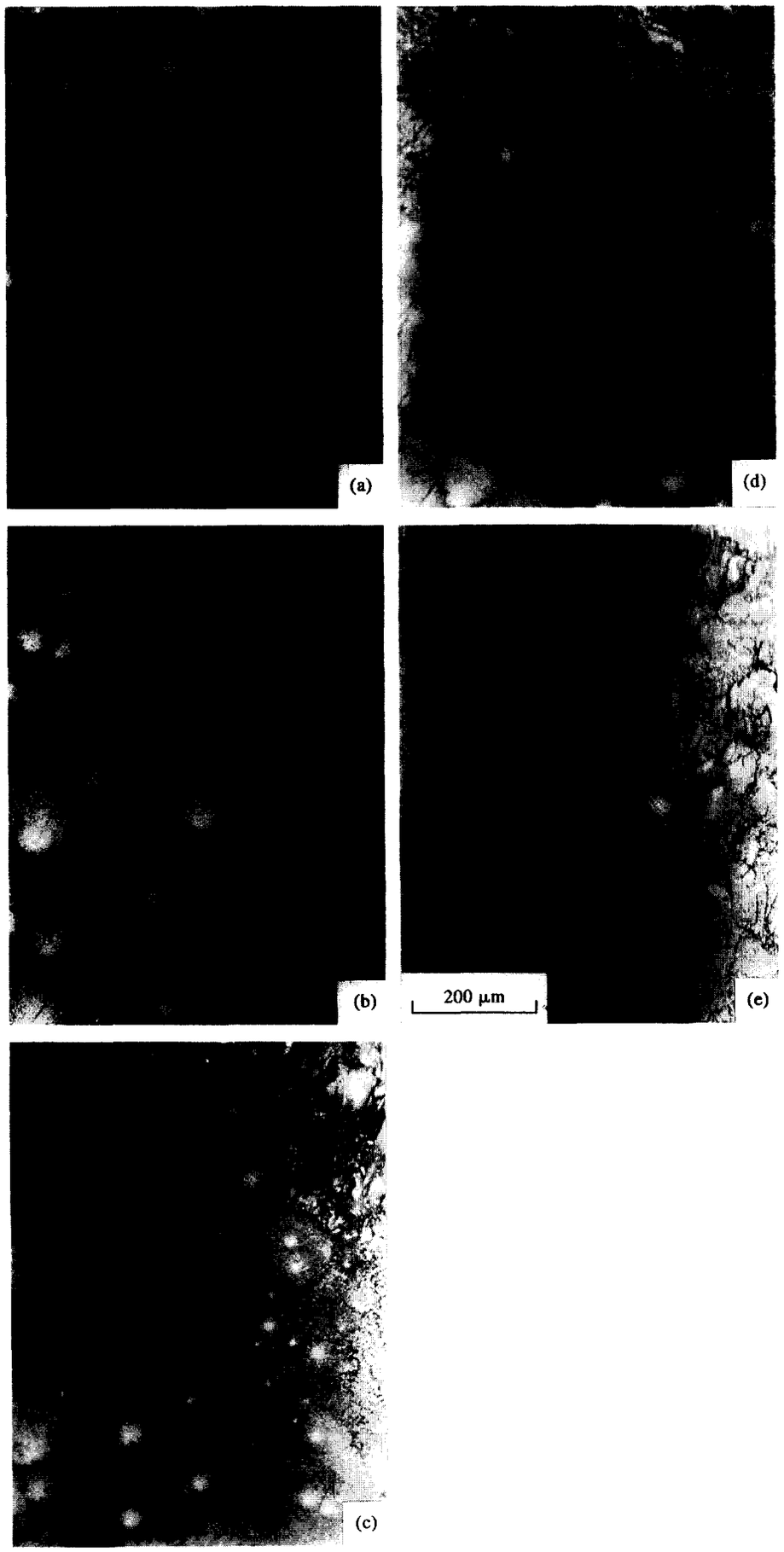

Figure 6 Fracture surface morphology of PMMA subjected to a tensile load with crosshead speeds of: (a) 0.22 mm min^{-1}, (b) 0.33 mm min^{-1}, (c) 0.44 mm min^{-1}, (d) 0.55 mm min^{-1} and (e) 0.66 mm min^{-1}

methanol mixed with chlorophyll as a function of the solvent treatment temperature is tabulated in *Table 1*. The dimple shape, as shown in *Figure 4a*, is redrawn schematically in *Figure 4e*. A comparison of *Figure 4e* with *Figure 3b* reveals that the final broken region of virgin PMMA is smaller than that in PMMA treated with chlorophyll. This implies that the effect of chlorophyll on fracture morphology is the most pronounced in region A. That is, when the methanol mixed with chlorophyll moves into PMMA, the chlorophyll concentration decreases from A to B to C. A reduction in the glass transition temperature, caused by the plasticizing effect of the methanol–chlorophyll mixture, subsequently leads to chain disentanglement. The chain resistance to the applied load is proportional to the degree of entanglement. Region A has a significant amount of residual chlorophyll so that the mechanical strength in region A is decreased and the final broken region becomes widened. Similarly, the degree of entanglement in regions B and C is low after chlorophyll treatment. As a result, the dimple in PMMA treated by chlorophyll is small and equiaxed instead of being large and parabolic, such as that in the virgin PMMA. An increase in the solvent treatment temperature causes an increase in the amount of residual chlorophyll. This subsequently leads to an increase in the degree of disentanglement. If some of the chains in region A disentangle and the degree of entanglement in region A

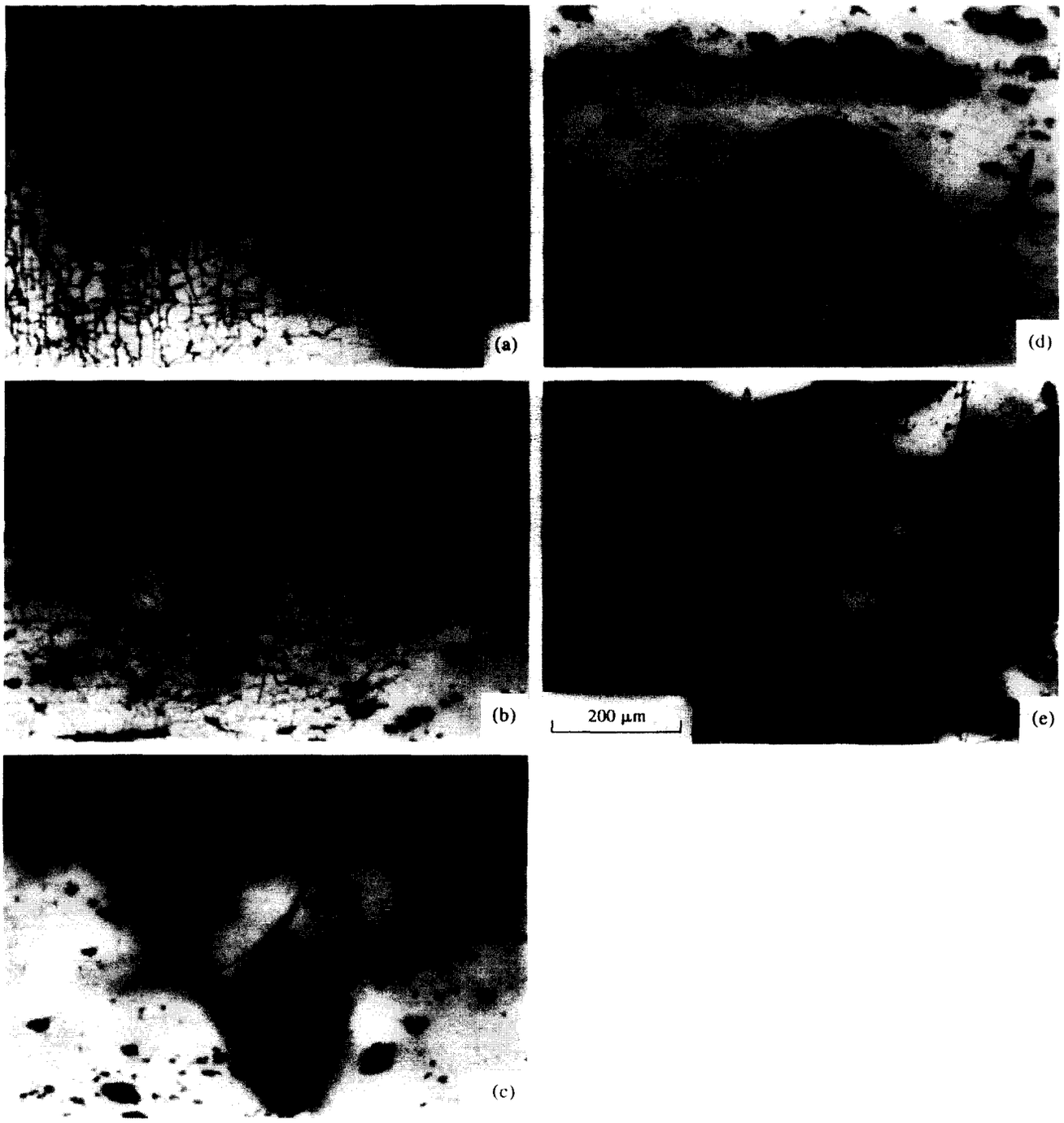

Figure 7 Optical micrographs of PMMA saturated with methanol at 40 C for various draw ratios: (a) 1.5, (b) 1.75, (c) 2, (d) 2.25 and (e) 2.5

almost resembles that in region B, the position of stress concentration in region B will also be at the final breaking point of the dimple under the action of an applied load. Therefore, the height of the dimple decreases with increasing temperature, and dimple density increases. When the temperature reaches 55°C, most of the chains disentangle so that no dimples are formed.

Gamma ray effects

The sample irradiated by gamma rays was fractured using a tensile machine with a crosshead speed of 0.66 mm min^{-1}. The fractographs of the PMMA irradiated with dosages of 10, 20 and 30 Mrad are illustrated in *Figures 5a, b* and *c*, respectively. The density of molecular chains after irradiation decreases in the order A > B > C. This decrease implies that the molecular chain cell is divided into two or more small cells. The higher the radiation dose, the larger the number of interpenetrating cells. Furthermore, a decrease in the molecular chain cell size leads to a small dimple. When the gamma ray dose is sufficiently high, the molecular chain cell is smaller than the critical size required to form dimples. Consequently, no dimples are observed on the fracture surface.

Strain rate effects

The sample after annealing was fractured using the tensile machine with various crosshead speeds. The fracture surface morphologies of PMMA are illustrated in *Figures 6a* to *e*, corresponding to crosshead speeds of 0.22, 0.33, 0.44, 0.55 and 0.66 mm min^{-1}, respectively. Also, the morphology for the sample deformed at a crosshead speed of 0.11 mm min^{-1} is shown in *Figure 3a*. An increase in crosshead speed causes a decrease in the dimple size. When the sample is under a tensile load, the straightening of chains starts in region C, and then B and, finally A. The chains are aligned along the tensile direction. The elongation of each region and the size of the dimple decrease with increasing crosshead speed for the same tensile load because molecular chains require time for their mechanical response. In addition, the elongation occurring in region C is extended to regions B and A as the crosshead speed increases. When the crosshead speed is sufficiently high, chains in each region have no time to elongate before breaking. Therefore, no dimples are observed. The fracture surface morphology corresponding to a high crosshead speed of 0.66 mm min^{-1} therefore shows many patches in *Figure 6e*.

Warm drawing effects

After immersion in methanol, the sample was observed using the Olympus BH-2 microscope with transmitted light. *Figures 7a–e* reveal the morphologies corresponding to the draw ratios 1.5, 1.75, 2, 2.25 and 2.5, respectively. As observed in *Figure 7*, voids are formed in region A for draw ratios >1.5. The size of the voids increases with draw ratio. In addition, cracks emanating from the void are observed for draw ratios of 1.5 and 1.75. At draw ratios of 2 and 2.25, a large void in region A resembles an eye and is accompanied by many small voids. The major axes of the eye and iris are perpendicular and parallel to the tensile direction, respectively. When the draw ratio is 2.5, the eye is fully occupied by the iris and small voids collapse to form a large void. Each large void is separated by white zones which resemble a river pattern.

During warm drawing, the molecular chains elongate along the tensile direction. Chains in region A are more difficult to elongate than those in region C. Therefore, the flow of chains in region A (slow motion) is accompanied by that in region C (fast motion). That is, the chain elongation in region C is greater than that in region A. Furthermore, after warm drawing region A has a larger residual stress than region C. Because the chains have larger residual stresses in region A than in region C, region A absorbs more methanol than region C. Therefore, when PMMA after warm drawing is immersed in methanol, chains in region A are easier to disentangle than those in region C. Once chains disentangle, voids are formed. This implies that region A is the most probable region where voids form.

SUMMARY AND CONCLUSIONS

A poly(methyl methacrylate) (PMMA) interpenetrating cell model has been proposed in this study based on the polymerization process. This model is concerned with the entanglement of molecular chains. The degree of entanglement is such that corner A > edge B > centre C. The PMMA was treated by various methods including mixtures of methanol with chlorophyll, gamma irradiation, crosshead speed variation, and warm drawing. The micrographs were compared with the model of the interpenetrating cell and the following conclusions can be made.

1. The tip, or last broken point, of the dimple occurs at region A. The dimple shape changes from a parabola to an equiaxial structure as the residual amount of methanol–chlorophyll mixture increases.
2. Gamma rays induce chain scission in PMMA so that the molecular chain cell is divided into smaller ones. The dimple size decreases with an increase in radiation dose; however, their population shows the opposite trend.
3. The tip location of the dimple extends from region A to region B as the crosshead speed increases. As a result, the dimple size decreases with increasing crosshead speed and their population increases.
4. Region A has the greatest residual stress so that it is the most probable region for void formation. The size of the void increases with the draw ratio.

REFERENCES

1 Chau, C. C. and Li, J. C. M. *Phil. Mag.* 1981, **A44,** 493
2 Harmon, J. P., Lee, S. and Li, J. C. M. *J. Polym. Sci.: Part A: Polym. Chem.* 1987, **25,** 3215
3 Harmon, J. P., Lee, S. and Li, J. C. M. *Polymer* 1988, **29,** 1221
4 Chapiro, A. 'Radiation Chemistry of Polymeric Systems', Interscience Publishers, Wiley, New York, 1962
5 Kusy, R. P. and Turner, D. T. *Polymer* 1977, **18,** 391
6 Lin, C. B., *Ph.D. Thesis*, National Tsing Hua University, Hsinchu, Taiwan, 1991
7 Kusy, R. P., Lee, H. B. and Turner, D. T. *J. Mater. Sci.* 1976, **11,** 118
8 Könczöl, L., Schirrer, R. and Döll, W. '27th Int. Symposium sur les Macromolecules', Strasbourg, 6–9 July 1981, Vol. II, p. 1050
9 Lin, C. B., Hu, C. T. and Lee, S. *Polym. Eng. Sci.* 1993, **33** (7), 431
10 Berry, J. M. *ASM Trans.* 1959, **51,** 556
11 Beachem, C. D. 'Fracture I' (Ed. H. Liebowitz), Academic Press, Boston, 1968, p. 243

12 Karel, V. *Z. Metallkunde* 1969, **60,** 298
13 Lin, C. B., Lee, S. and Liu, K. S. *J. Adhes.* 1991, **34,** 221
14 Broek, D. 'Elementary Engineering Fracture Mechanics', Martinus Nijhoff Publishers, Boston, MA, 1986, Ch. 2
15 Puttick, K. E. *Phil. Mag.* 1959, **4,** 964
16 Rogers, H. C. *AIME Trans.* 1960, **218,** 498
17 Lin, C. B., Lee, S. and Liu, K. S. *Polym. Eng. Sci.* 1990, **30,** 1399
18 Wang, P. P., Lee, S. and Harmon, J. P. *J. Polym. Sci.: Part B: Polym. Phys.* 1994, **32,** 1217
19 Flory, P. J. 'Principles of Polymer Chemistry', Cornell University Press, Ithaca, NY, 1953, Ch. IV